## Title
Electron butterfly distribution modulation by magnetosonic waves



## Journal
Geophysical Research Letters, 43(7)

## ISSN
0094-8276

## Authors
Maldonado, Armando A
Chen, Lunjin
Claudepierre, Seth G
et al.

## Publication Date
2016-04-16

## DOI
10.1002/2016gl068161

Peer reviewed

AGU PUBLICATIONS

Geophysical Research Letters

RESEARCH LETTER
10.1002/2016GL068161

**Key Points:**
- Unlike Berstein-mode waves, the observed waves are not bound by neighboring harmonics of the proton gyrofrequency
- Electron pitch angle distribution is modulated by the magnetosonic wave intensity
- Bounce resonance with magnetosonic waves is the mechanism behind our event's electron pitch angle distribution as shown by our simulation

**Correspondence to:**
A. A. Maldonado,
aam131130@utdallas.edu

**Citation:**
Maldonado, A. A., L. Chen, S. G. Claudepierre, J. Bortnik, R. M. Thorne, and H. Spence (2016), Electron butterfly distribution modulation by magnetosonic waves, *Geophys. Res. Lett.*, *43*, 3051–3059, doi:10.1002/2016GL068161.

Received 9 FEB 2016
Accepted 15 MAR 2016
Accepted article online 21 MAR 2016
Published online 14 APR 2016



# Electron butterfly distribution modulation by magnetosonic waves

**Armando A. Maldonado[1], Lunjin Chen[1], Seth G. Claudepierre[2], Jacob Bortnik[3], Richard M. Thorne[3], and Harlan Spence[4]**

[1]Department of Physics, University of Texas at Dallas, Richardson, Texas, USA, [2]Space Science Department, The Aerospace Corporation, El Segundo, California, USA, [3]Atmospheric and Oceanic Sciences Department, UCLA, Los Angeles, California, USA, [4]NASA Goddard Space Flight Center, Greenbelt, Maryland, USA

**Abstract** The butterfly pitch angle distribution is observed as a dip in an otherwise normal distribution of electrons centered about $\alpha_{eq} = 90°$. During storm times, the formation of the butterfly distribution on the nightside magnetosphere has been attributed to L shell splitting combined with magnetopause shadowing and strong positive radial flux gradients. It has been shown that this distribution can be caused by combined chorus and magnetosonic wave scattering where the two waves work together but at different local times. Presented in our study is an event on 21 August 2013, using Van Allen Probe measurements, where a butterfly distribution formation is modulated by local magnetosonic coherent magnetosonic waves intensity. Transition from normal to butterfly distributions coincides with rising magnetosonic wave intensity while an opposite transition occurs when wave intensity diminishes. We propose that bounce resonance with waves is the underlying process responsible for such rapid modulation, which is confirmed by our test particle simulation.

## 1. Introduction

Particles trapped in the Van Allen radiation belts undergo three quasiperiodic motions, from fastest to slowest: gyromotion around the field line, bounce motion between two mirroring points on the field line, and azimuthal drift around the Earth. Each motion is associated with an adiabatic invariant which is conserved for slow variation of the background magnetic field. Violation of the adiabatics can be caused by wave-particle interactions and can result in particles escaping through the magnetopause or along the field line and into the Earth's upper atmosphere. The nature of interaction between fast magnetosonic waves and electrons are of particular interest in this paper.

Fast magnetosonic waves are typically observed within a few degrees of the geomagnetic equator and are sometimes referred to as equatorial noise or ion Bernstein-mode waves. They are observed over a frequency range of a few hertz to a few hundred hertz confined between the proton gyrofrequency and the lower hybrid resonance frequency [*Russell et al.*, 1969]. Magnetosonic waves are magnetically compressional-mode waves that propagate nearly perpendicular to the background magnetic field and are generated through cyclotron harmonic instability due to energetic proton ring distributions (~10 keV) [*Boardsen et al.*, 1992; *Horne et al.*, 2000; *Chen et al.*, 2010]. Their dominant magnetic component points along the field line and has an average amplitude of about 50 pT [*Ma et al.*, 2013] but can occasionally be observed as high as 1 nT [*Tsurutani et al.*, 2014]. *Horne et al.* [2007] found that magnetosonic waves are capable of accelerating electrons in the outer radiation belt by Landau interaction.

During geomagnetic storms, electrons at all pitch angles are observed to be lost over a wide range of L shells, but the theory accounting for the loss of equatorially mirroring electrons ($\alpha_{eq}$=90°) is incomplete [*Shprits et al.*, 2008]. Electrons with mirror points exactly at the magnetic equator are exempt from gyroresonant interactions since they do not have a parallel velocity as required by the gyroresonant condition (except for ultrarelativistic energies). The electron butterfly pitch angle distribution is observed as a smooth dip in an otherwise normal distribution of electrons centered about $\alpha_{eq}$=90°. During storm times, this distribution has been attributed to global processes such as L shell splitting in tandem with other effects, namely, magnetopause shadowing or strong positive radial flux gradients [*Sibeck et al.*, 1987; *Su et al.*, 2010]. This occurs when drifting from nightside toward dayside, particles with higher pitch angles will drift to outer equatorial radial

locations in an asymmetric magnetic field. A recent study [*Xiao et al.*, 2015] presents an observation of the butterfly formation deep within the inner magnetosphere. In this paper it is suggested that Landau resonance interaction with MS waves and gyroresonant acceleration with chorus waves is a candidate mechanism. The combined scattering of magnetosonic waves and chorus waves, which operate at different local times, leads to the development of the butterfly distribution over a time scale of 9 h [*Xiao et al.*, 2015]. *Li et al.* [2016] showed that Landau resonance alone can lead to a butterfly distrbution. A paper by *Artemyev et al.* [2015] suggests that nonadiabatic scattering due to magnetic field deformation on the nightside can result in a butterfly distribution as well.

In this paper we present an event showing a close relationship between the electron butterfly distribution and magnetosonic waves simultaneously observed by Van Allen Probes, where the formation of butterfly distribution is modulated by the intensity of MS waves. Such local and rapid response of the butterfly formation is unlike all other processes previously mentioned, which leads us to promote another mechanism. The modulation observation is described in section 2. In section 3 we propose a new mechanism for the butterfly formation, which is confirmed through test particle simulations. Lastly, we summarize and discuss our findings in section 4.

## 2. Magnetosonic Wave Event and Butterfly Distribution Observation

Observations were made with the Van Allen Probes (formally known as the Radiation Belt Storm Probes). The two satellites have highly elliptical orbits of about ~0.1 to 5.8 Earth radii for their perigee and apogee, respectively, with low inclinations of 10° [*Mauk et al.*, 2013]. The Electric and Magnetic Field Instrument Suite and Integrated Science (EMFISIS) [*Kletzing et al.*, 2013] provides measurements of wave electric and magnetic field power spectral density up to 12 kHz and of DC magnetic field (MAG) with a sampling cadence of 64 vectors per second. Such sampling rate are used to obtain magnetosonic wave power spectral below 32 Hz (Nyquist theorem). The high-frequency receiver (HFR), another part of EMFISIS, measures spectral information between 10 and 400 kHz which provides the upper hybrid resonance frequency, from which the plasma density can be obtained. The Energetic Particle Composition and Thermal Plasma Suite (ECT) [*Spence et al.*, 2013] on board the Van Allen Probes consists of three highly coordinated instruments: the Helium Oxygen Proton Electron (HOPE) sensor, the Magnetic Electron Ion Spectrometer (MagEIS), and the Relativistic Electron Proton Telescope (REPT), covering electrons and ions over a broad energy range. The HOPE instrument [*Funsten et al.*, 2013] is designed to measure the full 3-D in situ plasma ion and electron fluxes over 1 eV to 50 keV energy range with logarithmical spacing. The proton measurement from HOPE are used to check the existence of proton ring distributions, which provides the free energy for magnetosonic wave excitation. The REPT instruments [*Baker et al.*, 2013] measures relativistic electrons in the energy range of ~2–20 MeV. The MagEIS instrument [*Blake et al.*, 2013] provides high-resolution energetic electron flux measurements with energy range of ~30–4000 keV. It contains four independent magnetic electron spectrometers on each spacecraft, one low-energy spectrometer, two medium-energy spectrometers (M75 and M35), and one high-energy spectrometer. In the normal mode of instrument operation electron pitch angle resolution is approximately 5°–10°. Each low- and medium-energy MagEIS unit can also be commanded into a high-angular resolution mode (the high unit does not utilize this high-angular resolution mode), resulting in a pitch angle resolution of approximately 1°–2° in this mode. This high-angular resolution data, which provides excellent detection of butterfly pitch angle distribution, will be used for our study.

The event of interest took place on 21 August 2013 at 06:00 UT. Figure 1 shows geomagnetic indexes and solar wind parameters over the five day period from 19 to 24 August. On 21 August, we observe moderate geomagnetic activity with $K_p \sim 4$ in Figure 1a and $AE \sim 800$ nT in Figure 1b. This is the initial phase of a weak storm where values of the *Dst* index in Figure 1c reach a minimum of about $\sim -30$ nT. The storm is associated with two shock encounters, one near the beginning of 21 August and the other toward the end of 21 August, which can be seen by enhanced solar wind density in Figure 1d and pressure in Figure 1f. The two shocks result in two bumps in *Dst* index. Solar wind speed changes gradually in Figure 1e, and the $B_y$ and $B_z$ components of interplanetary magnetic field in GSM coordinates flip their signs several times on 21 August. This may be a signature of a magnetic flux rope since the *B* field is rotating within the high-density region.

Figure 2 gives an observation of an MS wave event by Van Allen probe B over the interval from 06:00 to 08:00 UT. The MS event took place inside the plasmasphere near $L \sim 4.8$, ~17:00 MLT, and near a geomagnetic latitude of 1°. Figure 2a exhibits the magnetic field power spectral density from the EMFISIS onboard

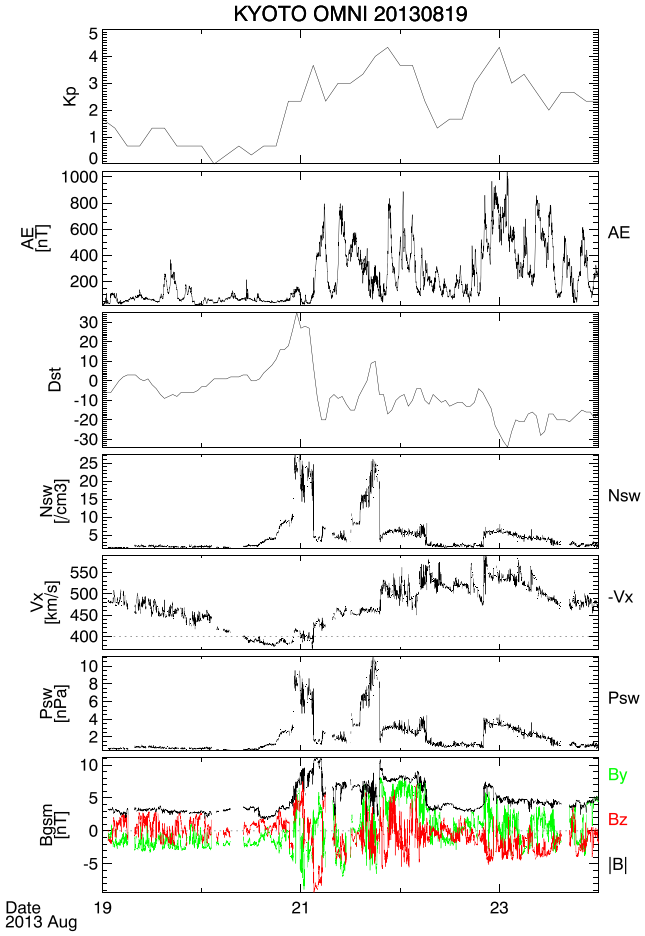


**Figure 1.** The 21 August 2013 storm event. Sudden storm onset is identified in the DST index at about 21:00 UT. (a) $K_p$ index. (b) *AE* index measured in nT. (c) $N_{sw}$ measured in $cm^{-3}$ by WIND satellite. (d) Solar wind speed in Sun-Earth direction measure in km/s. (e) $P_{sw}$ as solar wind pressure. (f) GSM magnetic field measurements.

FFT analysis where we notice most of the power resides below the lower hybrid resonance line with some weak hiss above the line. No chorus emission is seen during the interval. Figure 2b shows corresponding wave normal angles obtained from the singular value decomposition performed on board from EMFISIS. One can see an intensified magnetosonic waves emission in the interval between proton gyrofrequency $f_{CH}$ and the lower hybrid resonance frequency $f_{LHR}$ with nearly 90° wave normal angles. Despite the lower frequency resolution at lower frequency, the waves have significant power at frequency below 10 Hz. To resolve spectral properties at the low frequency, we use magnetic field vectors from the MAG data of EMFISIS, with 64 vectors per second, and perform windowed Fourier transforms to obtain the magnetic dynamic spectra. The spectra of the dominant component of magnetic field, the component parallel to the background magnetic field, are shown in Figure 2c, where the proton gyrofrequency is overlaid as a white dashed line and its harmonics as solid white lines. The wave emission below 32 Hz exhibits clear discrete lines which closely trace the proton gyrofrequency fundamental and harmonics. Additionally, there are five noticeable features.

1. The intense MS emission is initially detected near 06:20 with frequency near the first few harmonics.
2. The individual emission lines experience similar frequency shifts, maintaining the spacing of discrete lines about $f_{CH}$. One can see frequency rising (06:20–06:40), frequency falling near 06:40, and frequency oscillation (06:40–07:00). The constant frequency spacing of $f_{CH}$ suggests that the emission lies in the source region. This is consistent with proton phase space density at 90° pitch angles as a function of energy (Figure 2e), which is obtained from the HOPE measurement. One can see the availability of the free energy, proton ring distribution (i.e., inverse energy gradient) with ring velocity above local Alfvenic speed (magenta dashed line), which is calculated using the local magnetic field and plasma density from the upper hybrid resonance line.

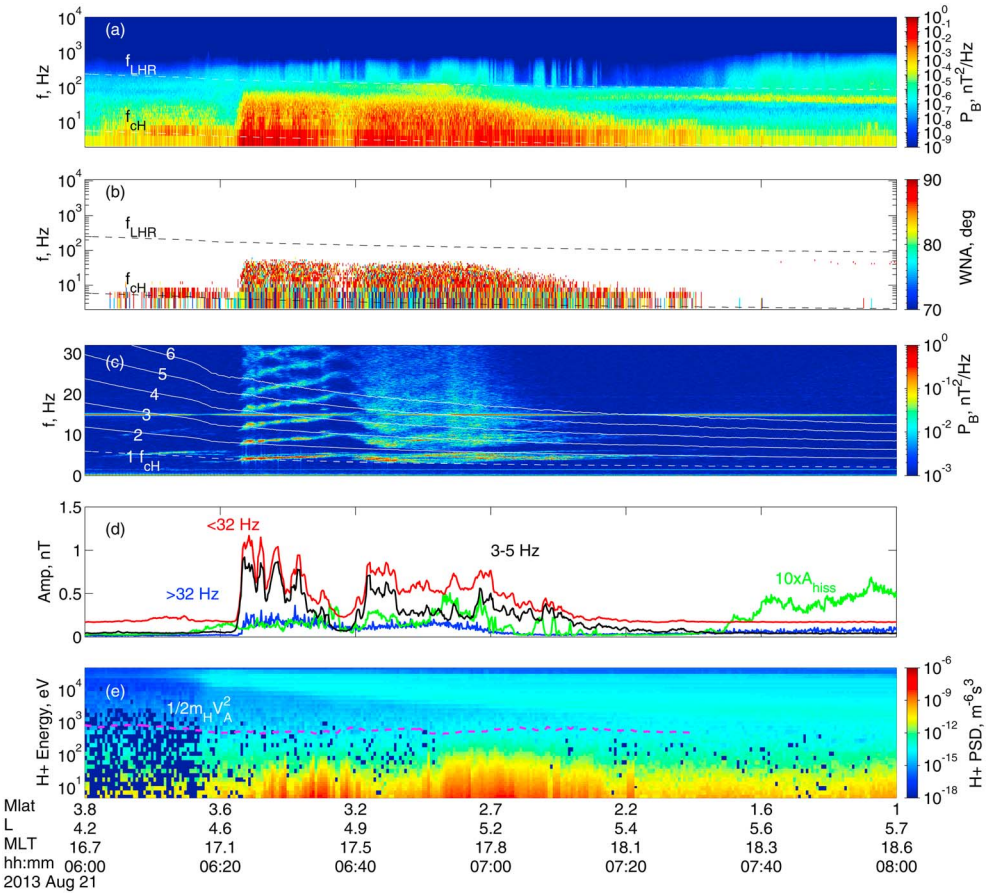


**Figure 2.** (a) Power spectral density analysis of the measured *B* field in nT$^2$/Hz taken from EMFISIS magnetic field data from Van Allen Probe B. (b) Wave normal angle in degrees for the observed wave. (c) Singular value decomposition of the wave measured in nT$^2$/Hz. The instrument measures at 64 Hz per second and therefore only presents the waves up to 32 Hz by Nyqvist theorem. Black lines in Figure 2 represent harmonics of the proton gyrofrequency. (d) Root-mean-square amplitude for the wave. Red represents frequencies <32 Hz, green for 3–5 Hz, blue for >32 Hz, and green for 10 times the hiss amplitude above $f_{LHR}$. (e) Proton phase space density. Red dashed line represents energy based on Alfvenic speed and proton energy.

3. An emission line is not necessarily limited by two neighboring $f_{CH}$ harmonics, unlike convectional ion Bernstein-mode dispersion relation. They can be away from multiples of $f_{CH}$, cross several $f_{CH}$ harmonics, and cross the same $f_{CH}$ harmonic multiple times.
4. There exists frequency broadening after 06:40, but coherent discrete emissions can be seen over 40 minutes.
5. There exists significant variation in wave intensity. This can be seen in the dynamic spectra in Figure 2a and 2c, and the root-mean-square amplitudes over different frequency ranges in Figure 2d. The smoothness of the harmonic lines indicates no corresponding rapid variation in the background magnetic field. No rapid variation of the plasma density is observed (not shown).

The red and black lines of Figure 2d represent the amplitudes below 32 Hz and between 3 and 5 Hz based on the spectrum in Figure 2c, respectively, the blue line represent the amplitude above 32 Hz and below $f_{LHR}$ based on the spectrum in Figure 2a, and the green line represents the hiss wave amplitude above $f_{LHR}$, which is scaled up by a factor of 10 since the hiss activity is weak. The MS wave is very intense with amplitude up to ~1 nT, much greater than the average amplitude 50 pT [*Ma et al.*, 2013]. One can also see that the majority of the wave power resides in waves below 32 Hz and most notably from 3 to 5 Hz. Large variation in wave amplitudes is clearly present, which is shown below to correlate well with electron pitch angle distribution variation.

Figure 3 shows the variability of pitch angle distribution of the electron count rate from the MagEIS with a high pitch angle resolution of about ~1° at various energy levels (31, 53, 78, 109, and 144 keV). The pitch angle

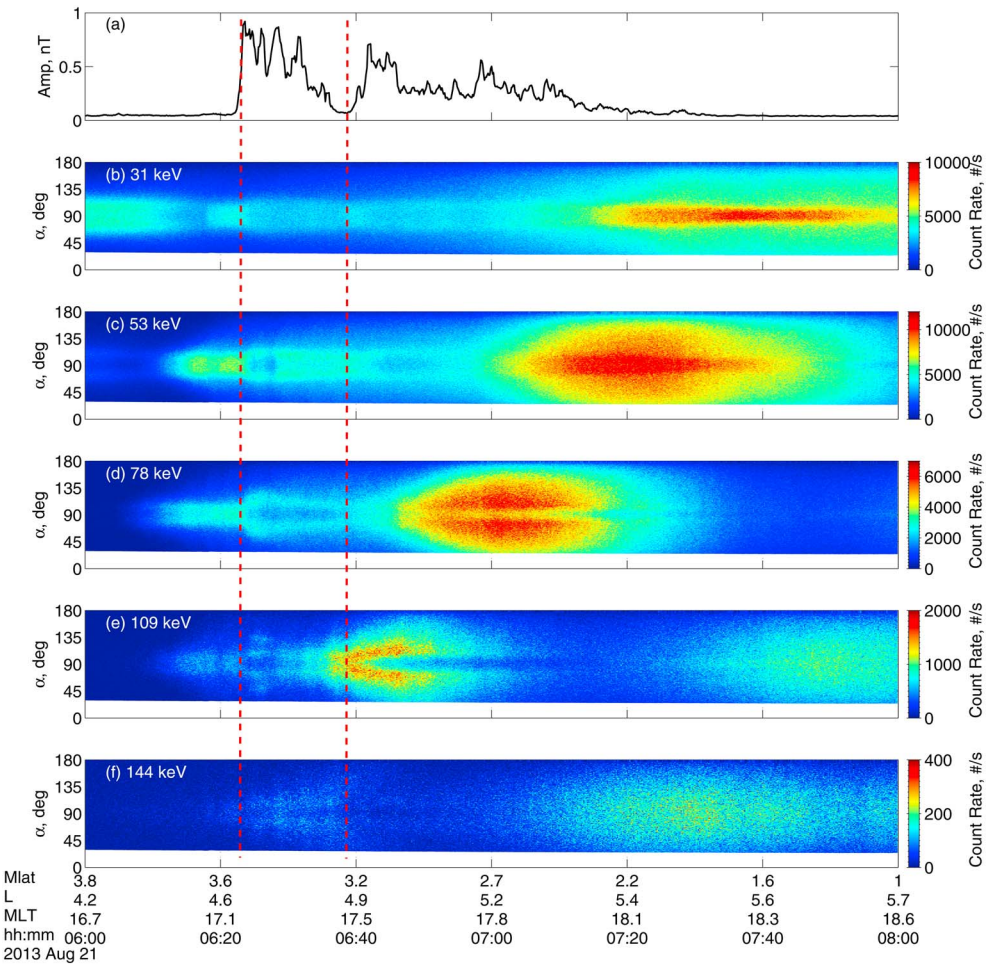


**Figure 3.** (a) Root-mean-square amplitude of waves magnetic field from 3 to 5 Hz. (b–f) Electron count rate for the local pitch angle distribution during the time interval of the MS wave event for energies of 31, 53, 78, 109, and 144 keV from the MagEIS observation on Van Allen Probe A.

is local to the satellite which means for a magnetic latitude of $\lambda = 3.5°$, a particle with a local pitch angle of $\alpha = 90°$ has an equatorial pitch angle of $\alpha_{eq} = 82.6°$. Since most of our wave power was from our 3–5 Hz range we chose the amplitude in this range as a reference (Figure 3a). Before the onset (~06:25) of the magnetosonic wave, a normal distribution centered about 90° is observed. At the immediate onset when the wave amplitude rises rapidly to ~1 nT within ~10 s, the electron counts with a pitch angle of 90° become significantly reduced for all presented energy levels while the count rate at lower pitch angles increase, resulting in a butterfly pitch angle distribution formation. Just as notable as the onset of the wave's amplitude, the first major dip in the magnetic amplitude (~06:35) of the wave corresponds to the disappearance of this butterfly formation most easily seen for 109 keV. Then as soon as the amplitude increases immediately after the dip, the butterfly PAD returns. As the wave vanishes at about 07:30, the PAD becomes normal again with a peak at $\alpha = 90°$. The close correlation between MS wave intensity and electron distribution excludes L shell splitting over a global drift motion as our primary mechanism. Such an immediate and local response of the electron distribution alone with the absence of chorus waves also excludes the combined effort of chorus and MS waves at different local times [*Xiao et al.*, 2015], which results in the development of the butterfly distribution over a time scale of hours. In addition, the lack of strong correlation between PAD modulation and weak hiss activity make it clear that the MS wave amplitude is rapidly modulating the electron PAD. It should be noted that the observed weak butterfly PAD before the most intense magnetosonic wave may be associated with weak magnetosonic waves whose first two harmonic lines are still visible in Figure 2c.

We propose the mechanism responsible for this event to be bounce resonance interactions with MS waves. Bounce resonance is thought to be important to the loss of equatorially mirroring electrons during

geomagnetic storms as suggested by *Parker* [1961] and *Roberts and Schulz* [1968]. The effect of violating the second invariant is also theoretically explored and described by *Chen et al.* [2015] and *Li et al.* [2015]. We will provide a test-particle simulation demonstrating the effect of bounce resonance for the electron butterfly distribution formation in the next section.

## 3. Bounce Resonance and Phase Space Simulation

Given the modulation of the electron pitch angle distribution by the magnetosonic wave intensity, a rapid and local mechanism is required. Thus, we look into the sole effect of magnetosonic waves on electron pitch angle distribution using a set of relativistic test particle equations following [*Bortnik and Thorne*, 2010; *Chen et al.*, 2015], where the effect of a monochromatic magnetosonic wave was studied. For the present study, the equations have been extended to multiple wave frequencies and are as follows:

$$\frac{\mathrm{d}p_z}{\mathrm{d}t} = -\frac{p_\perp^2}{2m_e B_0 \gamma}\frac{\partial B_0(z)}{\partial z} + \sum_j \sin\phi_j \left( J_1(\beta_j)\frac{eB_{x,j}p_\perp}{\gamma m_e} - J_0(\beta) eE_{z,j} \right) g(\lambda, t) \tag{1}$$

$$\frac{\mathrm{d}p_\perp}{\mathrm{d}t} = \frac{p_\perp p_z}{2m_e B_0 \gamma}\frac{\partial B_0(z)}{\partial z} - \sum_j \sin\phi_j J_1(\beta_j)(eB_{x,j}v_z + eE_{y,j}) g(\lambda, t) \tag{2}$$

$$\frac{\mathrm{d}\phi_j}{\mathrm{d}t} = \omega_j - k_{z,j}v_z \tag{3}$$

$$\frac{\mathrm{d}z}{\mathrm{d}t} = v_z, \tag{4}$$

where $t$ is time, $z$ is the distance along the field line measured from the equator with the Northern (Southern) Hemisphere taken as positive (negative), $p_z$ and $p_\perp$ are components of the electron's momentum parallel and perpendicular to the background magnetic field, $v_z$ is the parallel component of electron velocity, $e$ is the elementary charge, $m_e$ is the electron rest mass, and $\gamma$ is the electron Lorentz factor. Without loss of generality, we assume the wave vector **k** is contained in the $x$-$z$ plane so that **k**'s perpendicular component $k_\perp = k_x > 0$ and $k_z > 0$. The first terms on the right-hand sides of equations (1) and (2) represent the adiabatic effect of the background dipole magnetic field while the second terms represent the linear sum of forces due to multiple magnetosonic waves with the subscript $j$ denotes the $j$th wave component. Each wave has frequency $\omega_j$, parallel wave number $k_{z,j}$ and perpendicular wave number $k_{x,j}$ and wave phase $\phi_j$, wave magnetic field amplitudes $B_{x,j}$, $B_{z,j}$ and electric field amplitudes $E_{x,j}$, $E_{y,j}$, and $E_{z,j}$. Those amplitudes are linearly related through magnetosonic wave dispersion relation in an assumed cold magnetized plasma. The function $g(\lambda, t) = \exp(-\lambda^2/\delta\lambda^2)\exp(-(t - t_c)^2/\delta t^2)$ with three controlling parameters, the width of wave latitudinal distribution $\delta\lambda$, and temporal duration $\delta t$, the time $t_c$ corresponding to the peak wave power. $\delta t$ is set to 3 s and $t_c$ is set to 10 s in the simulation. Temporal variation is introduced to represent the turning on and off effect; the wave amplitude is initially off at $t = 0$ and when the test particle simulation is terminated (set to be $t = 20$ s), while wave amplitude maximizes at $t = 10$ s.

To examine the effect of magnetosonic waves on electrons, the magnetic field power spectrum is obtained through FFT analysis on three magnetic component measurement during a one-minute period from 06:23 to 06:24, corresponding to the maximum magnetic field power spectrum during the event. The low frequency range (3.5–4.5 Hz) of this power spectral intensity is shown as the blue line of Figure 4. A gaussian fit to this power spectral distribution is represented by red pluses. Since the observed harmonics have a finite width, we use 59 waves of discrete frequency in this range to represent the observed power spectral intensity corresponding to the first harmonic line, which contributes to most of the wave power. The dispersion relation for the waves are calculated using the magnetic field at the equator of $L = 4.8$ with the plasma density measurement ($N_e = 300$ cm$^{-3}$) derived from the upper hybrid resonance line of EMFISIS HFR spectrum. A constant wave normal angle of $\theta = 88°$ is adopted in the wave setup. Wave initial phases are randomly chosen.

Using the wave setup, we perform test particle simulations over 20 s for ~1.6 million electrons starting from the equator with different initial kinetic energy ($KE_0$), pitch angle ($\alpha_0$), and bounce phases. The following are chosen: 201 energies from 1 keV to 10 MeV with logarithmic spacing, 161 pitch angles from 10° to 90° with a spacing of 0.5°, and 48 equally spaced bounce phases over the range of $2\pi$. Figure 4b shows the pitch angle

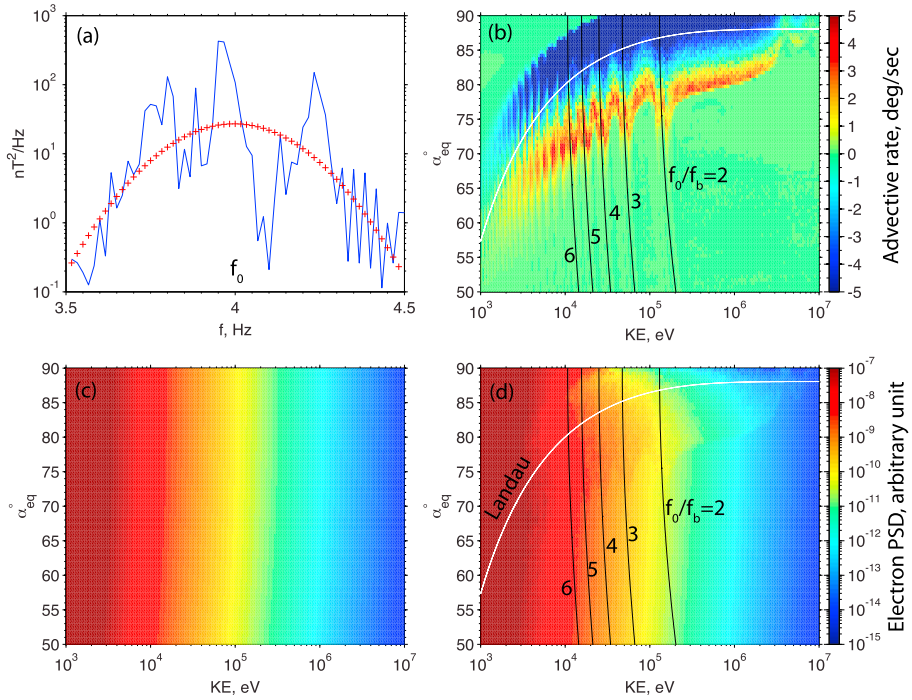


**Figure 4.** Simulation results. (a) Observed magnetic power spectrum FFT from MAG data on Van Allen probe A from 06:23 to 06:24 UT. Observations are blue, and the red line is a fitted normal distribution from 3.5 to 4.5 Hz centered about 4 Hz. (b) Color map of advection rate as a function of the initial equatorial pitch angle and electron energy from our simulation. The black dotted lines represent the lines of $f_0/f_b = 2, 3, 4, 5$. (c and d) The phase space density at $t = 0$ s and $t = 20$ s before and after the simulation, respectively.

advective response as a function of initial kinetic energy and pitch angle, defined as $< \alpha_{eq,f} - \alpha_{eq,f} >$, where $\alpha_{eq,f}$ and $\alpha_{eq,f}$ are initial and final equatorial pitch angles respectively and <> represent the averaging over the 48 bounce phases. One can see that strong negative pitch angle advection (toward lower pitch angles) is in effect for initially equatorially mirroring electrons over the energy range from ~30 keV to ~2 MeV and extends for lower pitch angle electrons at lower energy. Strong positive pitch angle advection (toward higher pitch angles) is seen in the pitch angles below those for the negative pitch angle advection. The white line represents the condition for Landau resonance with the center frequency ($f_c = 4$ Hz) while the black lines represents the condition of bounce resonances, $f_c = nf_b$, where $f_b$ is the bounce frequency and $n$ is an integer. One can see that both positive and negative pitch angle advection is the consequence of bounce resonance from examining the variation pattern of the advection and the condition of bounce resonance. To examine the phase space density evolution due to the effect of magnetosonic waves, given an initial phase space density $PSD_0(KE_0, \alpha_0) \sim KE_0^{-2} \sin^2 \alpha_0$ (Figure 4c), we assign each electron to represent a group of electrons in the corresponding energy and pitch angle bin with electron number determined by $PSD_0(KE_0, \alpha_0)$. With test particle simulation and Liouville theorem, which states PSD value along a particle trajectory is conserved the final $PSD_f$ can be constructed through rebinning in pitch angle and energy space (analogous to "particle in cell" simulation) and is shown in Figure 4d. One can see that pitch angle butterfly distribution, with peaks near ~80° forms at energies above tens of keV and up to a few MeV, which is fairly consistent with the observed characteristics. We also checked electron pitch angle distributions from REPT and found that the butterfly distribution, although at a much lower pitch angle resolution, is also visible for energy channels of 2, 2.3, and 2.9 MeV (not shown). The butterfly formation is a rapid response over the time scale of a few seconds (the effective magnetosonic wave driving time is about $2\delta t$). Negative pitch angle advection caused by bounce resonance leads to PSD reduction of near equatorially mirroring electrons (as observed in Figure 2). Further tuning of simulation parameters and increasing simulation time might yield better agreement, but our current simulation has already demonstrated the local and rapid response of electron distributions due to only MS waves through bounce resonance. One thing to note is that since the satellite is moving, we are not observing the same evolution of the temporal electron population. This makes it difficult to make a long term comparison between our simulation and observed data.

## 4. Conclusions and Discussion

We present an interesting event from Van Allen Probes where the electron pitch angle distribution is modulated by the intensity of the MS waves. The spectral properties of MS waves are examined, and the mechanism responsible for the modulation and for the formation of the electron butterfly distribution is proposed. A simulation for the mechanism is then provided. Our principal conclusions are summarized as follows:

1. An intense MS wave observation is presented. It contains discrete lines starting from the proton gyrofrequency $f_{CH}$ and exhibits frequency shifting. Unlike convectional ion Bernstein mode, the individual discrete lines are not bound by neighboring harmonics of $f_{CH}$.
2. Electron pitch angle distribution is modulated by the MS wave intensity. As the wave intensity rises, the electrons experience rapid transition from a normal distribution to a butterfly distribution. When the wave diminishes, the electron distribution returns to normal.
3. We proposed that bounce resonance with magnetosonic wave was the underlying mechanism to the local and rapid response of electron pitch angle distribution. Our test-particle simulation shows that bounce resonance can significantly decrease the phase space density of equatorially mirroring electrons and lead to rapid formation of butterfly distribution over a time scale of 20 s.

Both Landau resonance and bounce resonance with magnetosonic waves can affect electron dynamics. The observation of the electron pitch angle distribution modulated by the magnetosonic wave intensity demands a rapid mechanism. Landau resonance produces significant response of electrons for one bounce, but the effect of Landau resonance during the next bounce is likely independent of the previous bounce. This causes relatively slowly diffusive transport in pitch angle unless the bounce resonance condition is satisfied. Bounce resonance enables an accumulative effect over successive bounces, leading to a prompt and pronounced response of electrons. The negative advection in pitch angle near 90° caused by the bounce resonance can lead to the formation of a butterfly distribution on the order of 10 s. The bounce resonance requires coherent interaction over at least several bounce periods. The coherency of the observed emission is seen by the observation of clear discrete lines over about 1 h. For this event, slow diffusive processes like the combined effect of chorus and magnetosonic wave scattering and global processes like L shell splitting cannot explain the rapid electron response we observe. We also note that as the magnetosonic wave vanishes, the PAD does not immediately recover to a normal distribution, which can be accounted for by the fact that bounce resonance causes nonadiabatic changes in electron PAD.

Two factors assist in capturing the observed modulation of electron pitch angle distribution by magnetosonic wave intensity. One factor is high wave amplitude of magnetosonic waves associated with strong bounce resonance responses. The other factor is high pitch angle resolution of electron distribution, which allows us to resolve the change in pitch angle due to the bounce resonance effect. *Chen et al.* [2015] has shown that bounce resonance occurs when wave frequency matches bounce frequency harmonics, and it leads to removal of originally equatorially mirroring electrons out of the equatorial plane. It was also shown that the bounce resonance is in effect for weaker emission and the change of equatorial pitch angle tends to increase with increasing wave amplitude. For a weaker emission, the modulation effect might not be captured by in situ satellite. Detailed quantification of the bounce resonance effect on energetic electrons, for both equatorially and nonequatorially mirroring electrons, is left as future work.

**Acknowledgments**

MagEIS data were provided by the Aerospace Corporation. EMFISIS data were provided by NASA through spdf.gsfc.nasa.gov. We also acknowledge the use of OMNI data. This work was supported by NSF's Geospace Environment Modeling grant AGS1405041 and NASA's grant NNX15AF55G, NASA-LWS grant NNX13AI61G, and RBSP-ECT funding is provided by JHU/APL contract 967399 under NASA's Prime contract NAS5-01072. J.B. would like to gratefully acknowledge the support of NSF's Geospace Environment Modeling grant AGS-1103064.

## References

Artemyev, A. V., O. V. Agapitov, F. S. Mozer, and H. Spence (2015), Butterfly pitch angle distribution of relativistic electrons in the outer radiation belt: Evidence of nonadiabatic scattering, *J. Geophys. Res. Space Physics*, *120*, 4279–4297, doi:10.1002/2014JA020865.

Baker, D. N., et al. (2013), The Relativistic Electron-Proton Telescope (REPT) instrument on board the Radiation Belt Storm Probes (RBSP) spacecraft: Characterization of Earth's radiation belt high-energy particle populations, *Space Sci. Rev.*, *179*, 337–381, doi:10.1007/s11214-012-9950-9.

Blake, J., et al. (2013), The Magnetic Electron Ion Spectrometer (MagEIS) instruments aboard the Radiation Belt Storm Probes (RBSP) spacecraft, *Space Sci. Rev.*, *179*(1–4), 383–421, doi:10.1007/s11214-013-9991-8.

Boardsen, S. A., D. L. Gallagher, D. A. Gurnett, W. K. Peterson, and J. L. Green (1992), Funnel-shaped, low-frequency equatorial waves, *J. Geophys. Res.*, *97*, 14,967–14,976, doi:10.1029/92JA00827.

Bortnik, J., and R. M. Thorne (2010), Transit time scattering of energetic electrons due to equatorially confined magnetosonic waves, *J. Geophys. Res.*, *115*, A07213, doi:10.1029/2010JA015283.

Chen, L., R. M. Thorne, V. K. Jordanova, C. Wang, M. Gkioulidou, L. Lyons, and R. B. Horne (2010), Global simulation of EMIC wave excitation during the 21 April 2001 storm from coupled RCM-RAM-HOTRAY modeling, *J. Geophys. Res.*, *115*, A07209, doi:10.1029/2009JA015075.

Chen, L., A. Maldonado, J. Bortnik, R. M. Thorne, J. Li, L. Dai, and X. Zhan (2015), Nonlinear bounce resonances between magnetosonic waves and equatorially mirroring electrons, *J. Geophys. Res. Space Physics*, *120*, 6514–6527, doi:10.1029/2015JA021174.

Funsten, H., et al. (2013), Helium, Oxygen, Proton, and Electron (HOPE) mass spectrometer for the radiation belt storm probes mission, *Space Sci. Rev.*, *179*(1–4), 423–484, doi:10.1007/s11214-013-9968-7.

Horne, R. B., G. V. Wheeler, and H. S. C. K. Alleyne (2000), Proton and electron heating by radially propagating fast magnetosonic waves, *J. Geophys. Res.*, *105*, 27,597–27,610, doi:10.1029/2000JA000018.

Horne, R. B., R. M. Thorne, S. A. Glauert, N. P. Meredith, D. Pokhotelov, and O. Santolík (2007), Electron acceleration in the Van Allen radiation belts by fast magnetosonic waves, *Geophys. Res. Lett.*, *34*, L17107, doi:10.1029/2007GL030267.

Kletzing, C., et al. (2013), The Electric and Magnetic Field Instrument Suite and Integrated Science (EMFISIS) on RBSP, *Space Sci. Rev.*, *179*(1–4), 127–181, doi:10.1007/s11214-013-9993-6.

Li, X., et al. (2016), Formation of energetic electron butterfly distributions by magnetosonic waves via Landau resonance, *Geophys. Res. Lett.*, *43*, doi:10.1002/2016GL067853, in press.

Li, X., X. Tao, Q. Lu, and L. Dai (2015), Bounce resonance diffusion coefficients for spatially confined waves, *Geophys. Res. Lett.*, *42*, 9591–9599, doi:10.1002/2015GL066324.

Ma, Q., W. Li, R. M. Thorne, and V. Angelopoulos (2013), Global distribution of equatorial magnetosonic waves observed by THEMIS, *Geophys. Res. Lett.*, *40*, 1895–1901, doi:10.1002/grl.50434.

Mauk, B., N. Fox, S. Kanekal, R. Kessel, D. Sibeck, and A. Ukhorskiy (2013), Science objectives and rationale for the radiation belt storm probes mission, *Space Sci. Rev.*, *179*(1–4), 3–27, doi:10.1007/s11214-012-9908-y.

Parker, E. N. (1961), Effect of hydromagnetic waves in a dipole field on the longitudinal invariant, *J. Geophys. Res.*, *66*, 693–708, doi:10.1029/JZ066i003p00693.

Roberts, C. S., and M. Schulz (1968), Bounce resonant scattering of particles trapped in the Earth's magnetic field, *J. Geophys. Res.*, *73*(23), 7361–7376.

Russell, C. T., R. E. Holzer, and E. J. Smith (1969), OGO 3 observations of ELF noise in the magnetosphere: 1. Spatial extent and frequency of occurrence, *J. Geophys. Res.*, *74*, 755–777, doi:10.1029/JA074i003p00755.

Shprits, Y. Y., D. A. Subbotin, N. P. Meredith, and S. R. Elkington (2008), Review of modeling of losses and sources of relativistic electrons in the outer radiation belt II: Local acceleration and loss, *J. Atmos. Sol. Terr. Phys.*, *70*(14), 1694–1713, doi:10.1016/j.jastp.2008.06.014, dynamic Variability of Earth's Radiation Belts, AGU Fall Meeting.

Sibeck, D. G., R. W. McEntire, A. T. Y. Lui, R. E. Lopez, and S. M. Krimigis (1987), Magnetic field drift shell splitting: Cause of unusual dayside particle pitch angle distributions during storms and substorms, *J. Geophys. Res.*, *92*(A12), 13,485–13,497, doi:10.1029/JA092iA12p13485.

Spence, H. E., et al. (2013), Science goals and overview of the Radiation Belt Storm Probes (RBSP) Energetic Particle, Composition, and Thermal Plasma (ECT) suite on NASA's Van Allen probes mission, *Space Sci. Rev.*, *179*, 311–336, doi:10.1007/s11214-013-0007-5.

Su, Z., F. Xiao, H. Zheng, and S. Wang (2010), Combined radial diffusion and adiabatic transport of radiation belt electrons with arbitrary pitch angles, *J. Geophys. Res.*, *115*, A10249, doi:10.1029/2010JA015903.

Tsurutani, B. T., B. J. Falkowski, J. S. Pickett, O. P. Verkhoglyadova, O. Santolik, and G. S. Lakhina (2014), Extremely intense ELF magnetosonic waves: A survey of polar observations, *J. Geophys. Res. Space Physics*, *119*, 964–977, doi:10.1002/2013JA019284.

Xiao, F., C. Yang, Z. Su, Q. Zhou, Z. He, Y. He, D. N. Baker, H. E. Spence, H. O. Funsten, and J. B. Blake (2015), Wave-driven butterfly distribution of Van Allen belt relativistic electrons, *Nat. Commun.*, *6*, 8590.